RSC Advances

PAPER

View Article Online
View Journal | View Issue

Cite this: *RSC Adv.*, 2025, **15**, 17819

A calcium–copper-based zeolite with dual functions of hemostatic and antibacterial properties†

Mingtao Wang,[a] Yifeng Shi,[ab] Jianrong Huang,[a] Liping Xiao *[a] and Jie Fan *[a]

Wound treatment is a complex and lengthy process that involves rapid hemostasis in the early stage and the prevention of bacterial infection in the later stage. Generally, these two functions are separately achieved by different materials or medicines, thereby causing a lot of inconvenience and pain to patients. In this work, four calcium–copper-based zeolites (CaCuZ) with zeolite P, Y, X, and A structures were fabricated from corresponding sodium-based zeolites *via* ion exchange. Among these materials, the material with a zeolite P structure possesses better hemostatic performance than those with zeolite X and zeolite Y structures, and it shows improved antibacterial performance compared with the materials containing zeolite A and zeolite X structures. When the copper content of the CaCuZ material with the zeolite P structure is in the range of 0.64–6.30 mg g^{-1}, the clotting time of blood plasma is less than 2.5 min, the bacteriostasis rates against *Escherichia coli* (*E. coli*) and *Staphylococcus aureus* (*S. aureus*) are higher than 95%, and there is no obvious cytotoxicity towards 3T3 cells. A satisfactory balance in the clotting time, bacteriostasis, and cytotoxicity is achieved in this material, and the material integrates excellent hemostatic and antibacterial properties, offering great application prospects in wound treatment.

Received 2nd April 2025
Accepted 14th May 2025

DOI: 10.1039/d5ra02291f

rsc.li/rsc-advances

1. Introduction

Human injuries occur from time to time owing to various accidents. Wound treatment and care have long been a global health concern.[1–4] The healing of a severe wound is a complex and long process, generally including a hemostatic period, an inflammatory period, a proliferation period, and a remodelling period.[5–7] Hemostasis is the critical process in the early stage of wound treatment because failed hemostasis can be fatal. About 1.9 million people die every year worldwide because of uncontrollable hemorrhage.[8] Biological protein reagents, organic polymer materials such as natural polysaccharide chitosan, many kinds of lab-made hydrogels, as well as inorganic materials such as kaolin and zeolites have been developed as hemostatic materials.[9,10] Protein-based biological hemostatic materials are derived from coagulation factors, such as fibrinogen and thrombin, which possess excellent hemostatic performance but are limited by their extremely high cost and difficulties in usage, storage, transport, and distribution.[11] Chitosan and various organic hydrogels generally possess much higher stability and good biocompatibility. However, their efficiency in promoting blood coagulation is relatively low.[12–14] Among them, inorganic hemostatic materials, such as clay minerals (kaolin and montmorillonite), as well as synthetic and natural zeolites, are considered outstanding for their high efficiency in hemostasis and remarkably high stability.[15–21] Zeolites are a group of crystalline aluminosilicates with an ordered microporous structure.[22] Their well-developed porosity absorbs water from the blood to enable the rapid enrichment of coagulation factors.[23] Meanwhile, zeolites can absorb and assemble various coagulation factors on their surfaces to enhance prothrombin-to-thrombin conversion and accelerate the coagulation process.[24,25] The excellent hemostatic properties of zeolites have been widely recognized. However, most of the current hemostatic materials only have the function of hemostasis and cannot prevent wounds from bacterial infection during the long wound-healing process.

Bacterial infections, especially those caused by wound exposure, have been another major health problem for humans since ancient times. In 2019, nearly 7.7 million people died from bacterial infections.[26] The advent of has antibiotics greatly alleviated this problem. However, the abuse of antibiotics leads to bacteria easily developing resistance to them; consequently, the use of antibiotics is strictly restricted worldwide.[27] Compared with organic antibiotics, inorganic antibacterial materials such as copper, silver, and zinc can also kill bacteria while having a very small risk of causing bacterial resistance.[28] Therefore, inorganic antibacterial materials are allowed to be widely added into various daily products, such as the plastic

[a]*Key Lab of Applied Chemistry of Zhejiang Province, Department of Chemistry, Zhejiang University, Hangzhou 310027, China. E-mail: jfan@zju.edu.cn*

[b]*Hangzhou Zeolite-Innovation Life Science Technology Co., Ltd, Hangzhou 310018, China*

† Electronic supplementary information (ESI) available. See DOI: https://doi.org/10.1039/d5ra02291f

shell components of household appliances, wall coatings, and even children's clothing.

As one of the essential trace elements in the human body, copper has been used as an antibacterial agent since ancient times.[29,30] In 2008, copper was approved as a class 1 antibacterial metal.[31] It is generally believed that the antibacterial mechanism of copper involves depolarization of the bacterial cell membrane, resulting in cell membrane rupture.[32,33] Furthermore, it catalyzes the production of reactive oxygen species (ROS) to affect enzyme activity,[34,35] and induce deoxyribonucleic acid (DNA) damage.[36,37] Zeolites possess excellent ion exchange properties and can serve as carriers of copper ions to control their release, making copper-based zeolite a promising antibacterial agent.[38,39]

During the wound treatment process, it is necessary to stop bleeding and to prevent the wound from getting infected. Generally, multiple drugs are used step by step to meet the needs of wound treatment, which is inconvenient for patients. If a material possesses both hemostatic and antibacterial properties for wound treatment, it can stop bleeding and prevent bacterial infection, which is conducive to better wound healing and brings convenience to patients. Recently, a zeolite gauze with hemostatic and antibacterial properties through calcium and copper ion exchange has been reported.[39] However, the effects of different zeolite structures and copper ion contents on their hemostatic performance, antibacterial ability, and biocompatibility have not been carefully investigated and optimized.

In this work, we conducted calcium–copper ion exchange on four different structures of zeolites and performed a detailed study on the effects of zeolite structure and copper ions on their hemostatic and antibacterial properties. Meanwhile, zeolite can achieve a balance among hemostasis performance, antibacterial properties, and biocompatibility by optimizing the copper ion content. This type of bifunctional material can reduce the risk of bacterial infection during the early hemostasis process, bringing new hope for wound treatment.

2. Experimental section

2.1. Materials

Sodium-based zeolite Y (NaY), sodium-based zeolite X (NaX), and sodium-based zeolite A (NaA) were purchased from Tianjin Nanhua Catalyst Co., Ltd. Ludox HS-30 colloidal silica (30 wt% suspension in H_2O) was purchased from Hangzhou Chentong Biochemical Technology Co., Ltd. Calcium chloride (AR) was purchased from Sinopharm Group Chemical Reagent Co., Ltd. Copper nitrate trihydrate (AR) was obtained from Shanghai Maclin Biochemical Technology Co., Ltd. Bovine plasma was purchased from Chuzhou Shinorda Biotechnology Co., Ltd. *E. coli* CMCC (B) 44 102 was purchased from Shanghai Zhiqiao Biological Engineering Co., Ltd. *S. aureus* (ATCC25923) was purchased from China Medical Bacteria Preservation Management Center. Nutrition agar medium was purchased from Beijing Sanyao Technology Development Company. CCK8 reagent was purchased from Beyotime.

2.2. Preparation of CaCuZ

2.2.1. Synthesis of sodium-based zeolite P (NaP). NaP was prepared by a hydrothermal method from a precursor solution composed of 9 Na_2O : 0.7 Al_2O_3 : 10 SiO_2 : 331 H_2O.[40] Mixture (I) was prepared by dissolving sodium hydroxide and aluminum hydroxide in deionized water, and mixture (II) was prepared by mixing sodium hydroxide aqueous solution with colloidal silica (30 wt%). Then, mixture (I) was added dropwise into mixture (II) under vigorous stirring in an ice bath. The obtained clear solution was transferred into a hydrothermal reactor, and the hydrothermal treatment was carried out at 100 °C for 24 h. After the end of the hydrothermal process, the product was washed until neutral pH and dried at 100 °C to obtain NaP.

2.2.2. Calcium ion exchange of sodium-based zeolite (NaZ). NaZ (NaP, NaY, NaX, or NaA) was mixed with 5 M calcium chloride aqueous solution at a ratio of 0.2 g mL^{-1} with stirring at room temperature for 3 h. Then, the ion exchange solution was replaced with a fresh aqueous solution of 5 M calcium chloride of the same volume for another ion exchange cycle. Finally, the zeolite powder was washed, collected, and dried to obtain the corresponding calcium-based zeolite (CaZ), including calcium-based zeolite P (CaP), calcium-based zeolite Y (CaY), calcium-based zeolite X (CaX), and calcium-based zeolite A (CaA).

2.2.3. Copper ion exchange of CaZ. For each CaZ material, it was added into a copper nitrate aqueous solution using different concentrations (0.0001 M, 0.001 M, 0.01 M, 0.1 M, and 1 M) at a ratio of 0.2 g mL^{-1} with stirring at room temperature for 3 h. Then, the ion exchange solution was replaced with a fresh copper nitrate solution of the same concentration and same volume used in the first cycle for another ion exchange cycle. Subsequently, the zeolite was washed with deionized water, collected, and dried to obtain a CaCuZ sample that contains calcium and copper ions. The supernatant solution after each exchange was collected. Then, the concentration of copper ions in the solution was quantitatively detected using an ultraviolet spectrophotometer according to the method reported in the literature.[41] Thereafter, the adsorption amount of copper ions on each type of CaCuZ was calculated according to the following equation:

$$Q = \frac{(C_0 - C_e)\cdot V}{M}$$

where Q (mg g^{-1}) is the amount of copper adsorbed by CaCuZ, C_0 (mg L^{-1}) is the concentration of copper ions in solution before exchange, C_e (mg L^{-1}) is the concentration of copper ions in solution after exchange, V (L) is the volume of the solution, and M (g) refers to the quality of CaCuZ.

2.3. Characterizations

The surface morphology of the samples was observed and analyzed using a field-emission scanning electron microscope (SU8010, Japan). The X-ray diffraction patterns of the samples were recorded using an X-ray powder diffractometer (Ultima IV, Japan). The contents of Si and Al in the samples were analyzed using an X-ray fluorescence spectrometer (Panalytical Axios, the

Netherlands). The particle size and zeta potential of the samples were obtained using a laser particle size analyzer (LS13320, USA) and a nanoparticle size and zeta potential analyzer (Zetasizer Nano ZS, UK), respectively. The specific surface area and pore volume of the samples were obtained using a surface area and porosity analyzer (ASAP 2020 PLUS HD88, USA).

2.4. *In vitro* procoagulant ability evaluation of CaCuZ

2.4.1. *In vitro* plasma clotting assay. To ensure a common zero clotting time of the plasma, 50 μL of calcium chloride was added per 1 mL of plasma for recalcification. Five mg of zeolite was added into a 2 mL centrifuge tube. Then, 1 mL of plasma and the corresponding calcium chloride solution was added into the centrifuge tube at the same time to re-calcify the plasma. The clotting time recorded as the duration from the addition of the plasma into the tube to the clotting of plasma. The entire clotting measurement process was carried out in a 37 °C water bath.

2.4.2. Thromboelastography (TEG) analysis. Five mg of CaCuZ (copper ion exchange concentration: 0.01 M) was weighed into a specific cup and the cup was put into the thromboelasticity meter, followed by the addition of 340 μL of rabbit whole blood and 20 μL of 0.2 M calcium chloride to the cup, and the test was started at the same time. The relevant data were recorded and analyzed.

2.5. *In vitro* antibacterial evaluation of CaCuZ

2.5.1. *In vitro* antibacterial property. Activated *E. coli* and *S. aureus* were used as model bacteria in this work. First, the concentration of bacteria was adjusted to 10^4 CFU mL^{-1}. Then, the zeolite powder was added into the bacterial solution at a concentration of 0.5 mg mL^{-1}. After 6 h of oscillation in an incubator at 37 °C, the bacterial solution was removed and serially diluted, added to the agar plate, and counted after the colonies grew. The bacteriostasis rate was calculated using the following equation:

$$Y = \frac{(W_t - Q_t)}{W_t} \times 100\%$$

where Y is the bacteriostasis rate of the sample, W_t is the concentration of viable bacteria after 18 h in the control group (CaZ), and Q_t is the concentration of viable bacteria after 18 h in the experimental group.

After the antibacterial experiment, the bacterial solution was collected, and the bacteria were filtered out. Then, the concentration of copper ions in the solution was detected using an ultraviolet spectrophotometer with sodium diethyldithiocarbamate as the chromogenic agent.

2.5.2. Effect of CaCuZ on bacterial morphology. The four different CaCuZ (copper ion exchange concentration: 0.01 M) samples were added to a bacterial solution with a concentration of 10^7 CFU mL^{-1} at a ratio of 0.5 mg mL^{-1} for testing. Then, the bacteria were incubated at 37 °C for 6 h, washed with PBS, and fixed by adding 2.5% glutaraldehyde. Finally, the sample was dehydrated using different concentrations of ethanol, and the morphology change of the sample was observed using SEM.

2.6. Cytocompatibility of CaCuZ

The CaCuZ material was immersed in serum-free Dulbecco's modified Eagle's medium (DMEM) at a ratio of 200 μg mL^{-1}, leached at 37 °C for 24 h, and the sample extract was filtered using a filter membrane (pore size 0.22 μm). 3T3 cells were inoculated in 96-well plates at a density of 10 000 cells per well. After cell adhesion, the original culture medium was removed, and 100 μL of sample extract was added. Serum-free DMEM culture medium was added to the negative control group, and serum-free DMEM culture medium without cells was added to the positive control group. At least four replicates were used for each group. After 24 h, the extract was removed, CCK8 reagent was added, and it was reacted for 3 h. The absorbance of the solution at 450 nm was measured using a microplate reader. The relative cell survival rate was calculated using the following equation:

$$\text{Cell viability}(\%) = \frac{\text{Abs(sample)} - \text{Abs(blank)}}{\text{Abs(control)} - \text{Abs(blank)}} \times 100\%$$

where Abs (sample) is the absorbance of the experimental group, Abs (blank) is the absorbance of the positive control group, and Abs (control) is the absorbance of the negative control group.

3. Results and discussion

3.1. Preparation and characterization of CaCuZ

NaP zeolite was synthesized using a hydrothermal synthesis method at 100 °C for 24 hours and it exhibited bayberry morphology (Fig. S1a†). Its XRD pattern was consistent with that of standard NaP zeolite (Fig. 1a), indicating that well-crystallized NaP zeolite was successfully synthesized. The XRD analysis demonstrated that all the CaCuZ products possess the same crystal structure as their NaZ precursors (Fig. 1), indicating that the inorganic zeolites were stable as expected. The main characteristic diffraction peak intensities of all CaCuZ materials are slightly lower than those of their corresponding precursor NaZ materials, which can be explained by the heavy atoms like Ca and Cu absorbing more X-rays, and the introduction of high-valent metal ions alters the electron density distribution of the zeolite framework. The particle morphologies of commercially purchased NaY, NaX, and NaA were octahedral, octahedral, and cubic, respectively (Fig. S1†), which could be attributed to their different crystal structures. The Si/Al ratios of NaP, NaY, NaX, and NaA were calculated from the composition data measured by XRF analysis, which were 1.99, 3.22, 1.48, and 1.66, respectively, as shown in Table S1.† The average particle sizes of NaP, NaY, NaX, and NaA were approximately 12.2, 1.9, 5.5, and 2.9 μm, respectively and the particle size distribution profiles remained unchanged after the ion exchange treatment (Fig. S2†). The zeta potentials of the four types of NaZ were all around −40 mV, indicating that the surfaces of NaZ all carried negative charges. The zeta potentials of CaCuZ materials are all slightly higher than that of their corresponding NaZ materials, but still less than −35 mV (Fig. S3†). The N_2 adsorption and desorption analysis results

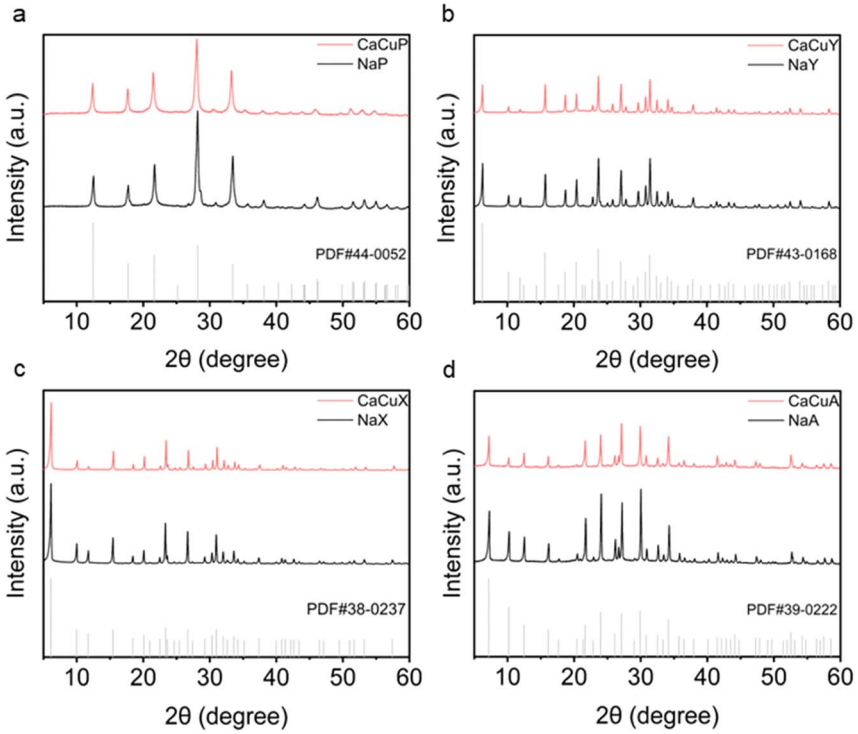

Fig. 1 XRD patterns of (a) calcium–copper-based zeolite P (CaCuP), (b) calcium–copper-based zeolite Y (CaCuY), (c) calcium–copper-based zeolite X (CaCuX), and (d) calcium–copper-based zeolite A (CaCuA) fabricated using 0.01 M copper ion exchange solutions, and their NaZ precursors.

showed that the specific surface areas of zeolite P and zeolite A were much smaller than those of zeolite Y and zeolite X, but the pore volumes of zeolite P and zeolite A were larger than those of zeolite Y and zeolite X (Table S2†).

CaZ materials (including CaP, CaY, CaX, and CaA) were fabricated from the corresponding NaZ materials using a calcium ion exchange treatment and 5 M $CaCl_2$ aqueous solution as the calcium ion source. After this treatment, almost all sodium ions were replaced by calcium ions due to the high concentration of the $CaCl_2$ aqueous solution and the repeated ion exchange process. It has been reported that a high calcium content can improve the hemostatic performance of zeolite materials without introducing cytotoxicity.[42] Afterward, each type of CaZ material was separately exchanged with a series of $Cu(NO_3)_2$ solutions of different concentrations to obtain CaCuZ with different copper content. The amount of copper adsorbed by CaZ material was calculated by measuring the residual copper amount in the ion exchange solution using ultraviolet spectrophotometry, and the results were listed in Table 1.

Table 1 Adsorption of copper by zeolites at different copper ion exchange concentrations

Copper ion exchange concentration (M)	Q (mg g^{-1})			
	CaCuP	CaCuY	CaCuX	CaCuA
0.0001	0.06	0.06	0.06	0.06
0.001	0.64	0.64	0.64	0.64
0.01	6.3	6.3	6.3	6.3
0.1	26.67	30	44.33	49.33
1	66.67	70	136.67	176.67

It was found that CaZ adsorbed almost all copper ions in the ion exchange solution when the concentration of copper ions was 0.0001 M, 0.001 M, and 0.01 M. Consequently, the corresponding copper content of CaCuZ samples with different crystal structures was the same in these cases. When the concentration of copper ions was increased to above 0.01 M, CaX and CaA adsorbed significantly more copper than CaP and CaY, which may be ascribed to the difference in their crystal structure and the Si/Al ratio. Zeolite X and zeolite A possessed significantly lower Si/Al ratios (1.48 and 1.66), which means that they have higher ion exchange capacities.

3.2. *In vitro* procoagulant ability evaluation of CaCuZ

The procoagulant activities of CaCuZ materials were evaluated through a conventional *in vitro* plasma coagulation experiment according to a procedure reported elsewhere.[40] The plasma clotting time of the control group was adjusted to 10.1 ± 0.2 min by adding appropriate $CaCl_2$ aqueous solution to recalcify the plasma, which had been anticoagulated with citrate phosphate for long-term storage. The clotting times of CaP, CaY, CaX, and CaA materials without copper ions were 101, 107, 110, and 103 s, respectively, indicating a high efficiency of procoagulation for these zeolites (Fig. 2a and b). These materials showed similar procoagulation performance, although they have different crystal structures, particle morphologies and sizes, and Si/Al ratios.

When the CaZ materials were further loaded with copper ions, the plasma clotting time increased with higher copper content; *i.e.*, the copper content will evidently affect the hemostatic performance. When the copper content of CaCuZ reached 6.30 mg g^{-1}, the plasma clotting time of CaCuP, CaCuY, CaCuX, and CaCuA slightly increased to 107, 116, 131, and 109 s, respectively, which can still be considered as excellent hemostatic materials (Fig. 2b). Zeolite P and zeolite A showed relatively better performance than zeolite Y and zeolite X, and zeolite X possessed the longest plasma clotting time among these four zeolites. The further increase in the copper content leads to a significant increase in plasma clotting time, even longer than 7 min. CaCuP showed much better resistance to copper ion interference, and its clotting time was shorter than

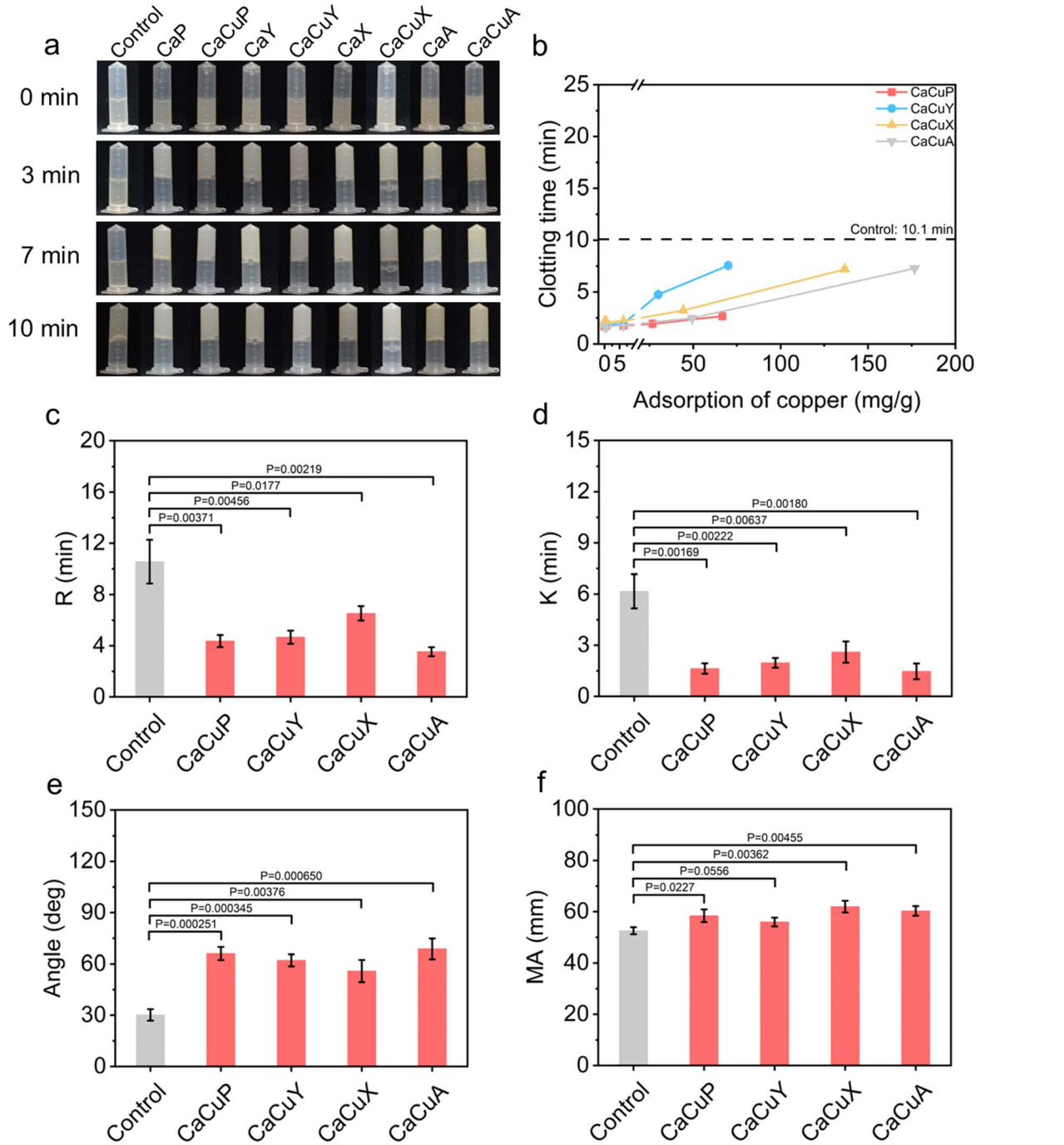

Fig. 2 (a) Photographs of the blank control, CaZ, and CaCuZ (adsorption of copper: 6.30 mg g^{-1}) in the *in vitro* plasma clotting assay. (b) Plasma clotting time of CaCuZ with different adsorption amounts of copper. (c) Coagulation reaction time (*R*-value), (d) blood clot formation time (*K* value), (e) solidification angle (α value), and (f) maximum amplitude (MA value) of the control sample and CaCuZ zeolite samples with a copper content of 6.30 mg g^{-1} obtained from TEG analysis. Data values correspond to mean ± standard deviation (SD), $n = 3$. Error bars represent SD. Analysis was performed using one-way analysis of variance (ANOVA).

3 min in all tests, indicating that it still possesses excellent procoagulation properties with a high copper content. The above results clearly demonstrated that the introduction of copper ions will affect the procoagulation performance of these zeolites.

It has been reported that the negatively charged inorganic surface can promote the activation of coagulation factor XII, thereby accelerating the coagulation process.[43,44] The strong negatively charged surface of these zeolites indicated by their zeta potential analysis results implies that they can efficiently activate factor XII, and thereby promote blood coagulation. When copper ions were introduced into zeolite, the surface charge density slightly decreased, as shown in Fig. S3,† which may affect its efficiency in activating coagulation factor XII. This may be one of the reasons why the procoagulant performance of each CaCuZ was weaker than that of the corresponding CaZ material.

The procoagulant activities of different types of CaCuZ samples with 6.30 mg g^{-1} copper content were also evaluated using a thromboelastometer. The *R*-values of all four CaCuZ samples were significantly smaller than that of the control group, in which no inorganic materials were added to the blood, indicating that all CaCuZ samples can apparently speed up the initiation stage of the coagulation process (Fig. 2c). Compared with the control group, CaCuZ samples had a smaller *K* value and a larger α value, indicating that CaCuZ can accelerate the transformation of fibrinogen to fibrin (Fig. 2d and e). In addition, CaCuZ had a larger MA value, indicating that CaCuZ can enhance the strength and stability of blood clots (Fig. 2f). Together, these results confirmed that all these CaCuZ materials possess excellent hemostatic properties as expected when the copper content was approximately 6.30 mg g^{-1}. Among these four different zeolites, CaCuP and CaCuA gave smaller *R* and *K* values, and larger α values than those of CaCuY and CaCuX, indicating a better performance in procoagulation. This result was consistent with the above-described plasma clotting time measurements.

3.3. The effect of copper on plasma coagulation

As demonstrated above, a higher copper content could significantly prolong the clotting time of a material; *i.e.*, it seems copper ions will inhibit plasma coagulation. This phenomenon was reported in the literature, but the reason has not been investigated.[45] Among all these four zeolites, the CaCuP and CaCuA materials showed a slower increasing trend in clotting time with the rise of copper content (Fig. 2b), and the CaCuX and CaCuA materials showed much steeper slopes. Surprisingly, it seems that the CaCuY samples were much more sensitive to copper content. The huge difference clearly indicated that the crystal structure does affect the resistance to copper ion interference. From the perspective of copper absorption capability, CaY zeolite and CaP zeolite were quite similar, and the absorption amounts of both were significantly less than that of CaX and CaA zeolites, especially in the high concentration conditions, which can be explained by the difference in their Si/Al ratios. However, CaY was dramatically affected by copper ions, as shown in Fig. 2b while CaP possessed much better resistance. From this, we can infer that the adsorption capacity of zeolite for copper is not the key reason for the hemostatic ability of zeolite.

Based on this situation, we compared the effect of copper ions on the plasma clotting time with and without the presence of zeolite. Different amounts of copper nitrate aqueous solution were added into the plasma to achieve different copper ion concentrations in the plasma. Then, the clotting time was measured for the control group and CaCuZ samples with 6.30 mg g^{-1} copper content. The results showed that the plasma clotting time increased exponentially in the control group with higher amounts of copper added (Fig. 3), while the increase in the plasma clotting time for CaCuZ samples was quite insignificant. For example, the plasma clotting time of the control group was 115.5 $\pm$ 1.8 min when the copper concentration of the plasma was 45 ppm, while the plasma coagulation time of CaCuP, CaCuY, CaCuX, and CaCuA was 2.1 $\pm$ 0.01 min, 2.4 $\pm$ 0.05 min, 2.5 $\pm$ 0.07 min, and 2.2 $\pm$ 0.06 min, respectively (Fig. 3).

These results confirmed that copper ions can significantly inhibit plasma coagulation as reported in the literature.[45] However, the presence of zeolite can be a huge buffer pool for copper ions, which decreases the copper ion concentration of the plasma and diminishes the impact of copper ions on coagulation. In other words, the copper ions staying within plasma can significantly affect the coagulation process, while the copper ions that are absorbed and confined inside the zeolite have little effect on the coagulation process. Therefore, the copper leaching amount should be the key reason affecting the procoagulation performance of the CaCuZ materials. The results suggested that CaCuY and CaCuX may release more copper ions when they come into contact with plasma. However, it is hard to separate the fine zeolite powder from the plasma clot to test the copper ion concentration of the plasma. We will investigate the copper-leaching behavior of these CaCuZ materials in subsequent experiments.

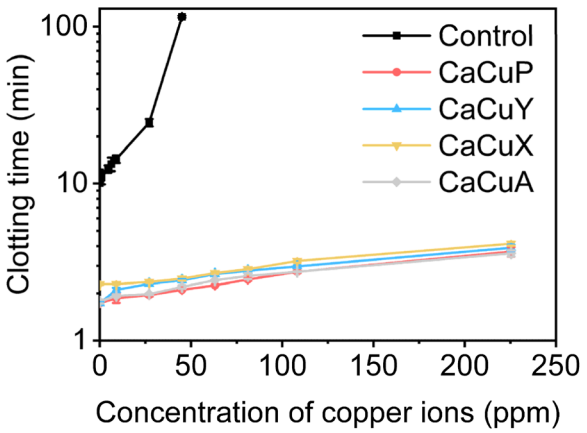

Fig. 3 Plasma clotting time of the control group without zeolites and the CaCuZ (adsorption of copper: 6.30 mg g^{-1}) group with different concentrations of copper ions in the plasma. Data values correspond to mean $\pm$ standard deviation (SD), $n = 3$. Error bars represent SD.

3.4. *In vitro* antibacterial evaluation of CaCuZ

The antibacterial performances of CaCuZ zeolites with different crystal structures were evaluated using a conventional oscillating method as reported elsewhere.[39] The antibacterial properties of zeolites could be directly observed through their colony photos (Fig. 4a, b, S4 and S5†). The results showed that the bacteriostasis rates of CaCuP, CaCuY, CaCuX, and CaCuA against *E. coli* were 88.5 ± 2.8%, 91.7 ± 2.2%, 84.2 ± 2.8%, and 30.7 ± 10.7%, respectively when the copper contents of the CaCuZ zeolites were very small (0.06 mg g^{-1}) (Fig. 4c); meanwhile, the bacteriostasis rates against *S. aureus* were 85.0 ± 4.3%, 97.3 ± 0.88%, 10.6 ± 9.5%, and 9.3 ± 5.3%, respectively (Fig. 4d). In both cases, CaCuA obviously gave the lowest bacteriostasis rates, while CaCuY gave the highest bacteriostasis rates among the other zeolites. With the increase in the copper contents of CaCuZ zeolites, the antibacterial properties of all four materials increased. When the copper content of CaCuP and CaCuY reached 0.64 mg g^{-1}, the bacteriostasis rate against *E. coli* and *S. aureus* was >95%, while the copper content needed to increase to above 6.30 mg g^{-1} for CaCuX and CaCuA zeolites to achieve the same antibacterial level (>95%). This indicated that CaCuP and CaCuY showed much better antibacterial properties than CaCuX and CaCuA zeolite with the same copper content.

The concentrations of copper ions released by CaCuZ during the antibacterial process were measured by ultraviolet spectrophotometry. As shown in Fig. 4e, the concentration of copper ions released by CaCuZ rose as the amount of copper absorbed by CaCuZ increased. The concentration order of the release of copper ions from highest to lowest was CaCuY > CaCuP > CaCuX > CaCuA, which was consistent with the order of their antibacterial ability. This result suggested that the abilities of zeolites to release copper ions affect their antibacterial properties. It should be noted that although zeolite X and zeolite A had much higher copper contents (137 mg g^{-1} and 177 mg g^{-1}), they still released less copper ions than those of zeolite P and zeolite Y with 67 mg g^{-1} and 70 mg g^{-1} copper content, respectively which should be ascribed to the higher affinity of copper ions by CaCuA and CaCuX.

3.5. Effect of CaCuZ on bacterial morphology

The effect of CaZ and CaCuZ on the morphology of bacteria was observed by scanning electron microscopy using CaCuZ zeolites with 6.30 mg per g copper content as examples. As shown in Fig. 5, the bacteria were colored to distinguish zeolite from bacteria (the original SEM image without color was shown in Fig. S6†). *E. coli* and *S. aureus* maintained complete cell morphology after contact with all four CaZ zeolites, indicating that they did not cause damage to these bacteria. On the contrary, the cell membranes of *E. coli* and *S. aureus* were significantly dented and severely damaged by CaCuZ zeolite. This result further indicated that CaCuZ has excellent antibacterial properties.

3.6. Cytocompatibility of CaCuZ

The biocompatibilities of the four CaCuZ materials were evaluated using a typical cytotoxicity assay, and the experimental scheme was improved by referring to the previous experiment.[46] Overall, the results showed that with an increase in copper content in CaCuZ, the cell survival rate of zeolites decreased, which can be ascribed to the enhanced leaching of copper ions

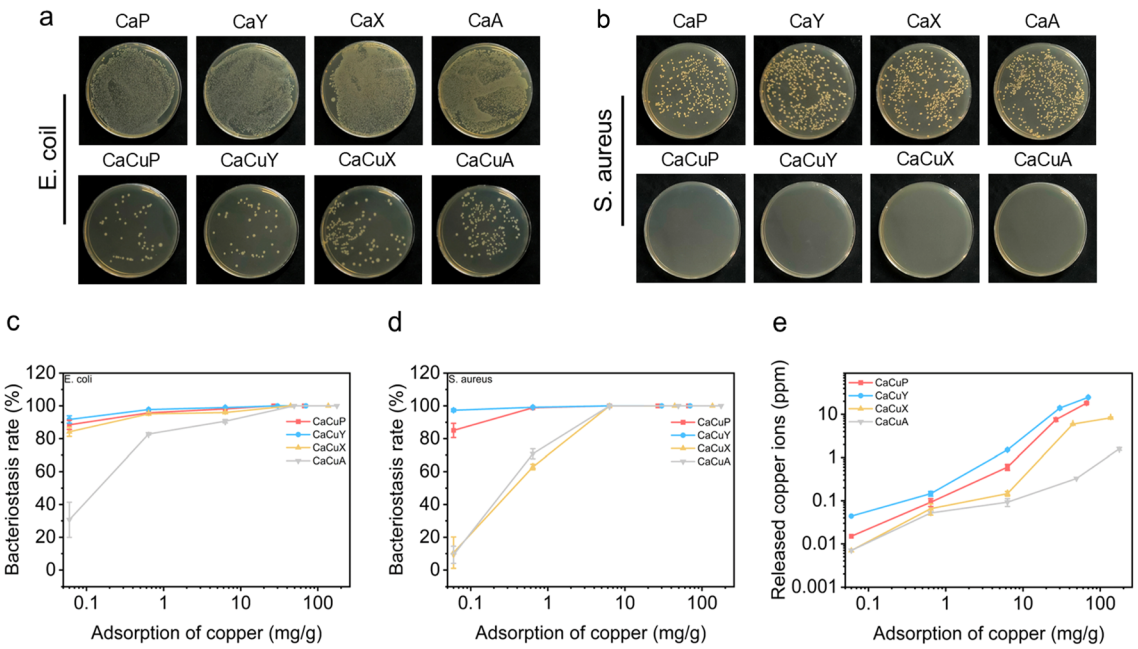

Fig. 4 Photographs of (a) *E. coli* and (b) *S. aureus* colonies treated with CaZ and CaCuZ with a copper content of 6.30 mg g^{-1}. Bacteriostasis rates of CaCuZ against (c) *E. coli* and (d) *S. aureus* with different adsorption amounts of copper. The data correspond to mean ± SD error bars, $n = 3$. (e) The concentration of copper ions released by CaCuZ with different adsorption amounts of copper during the antibacterial assay.

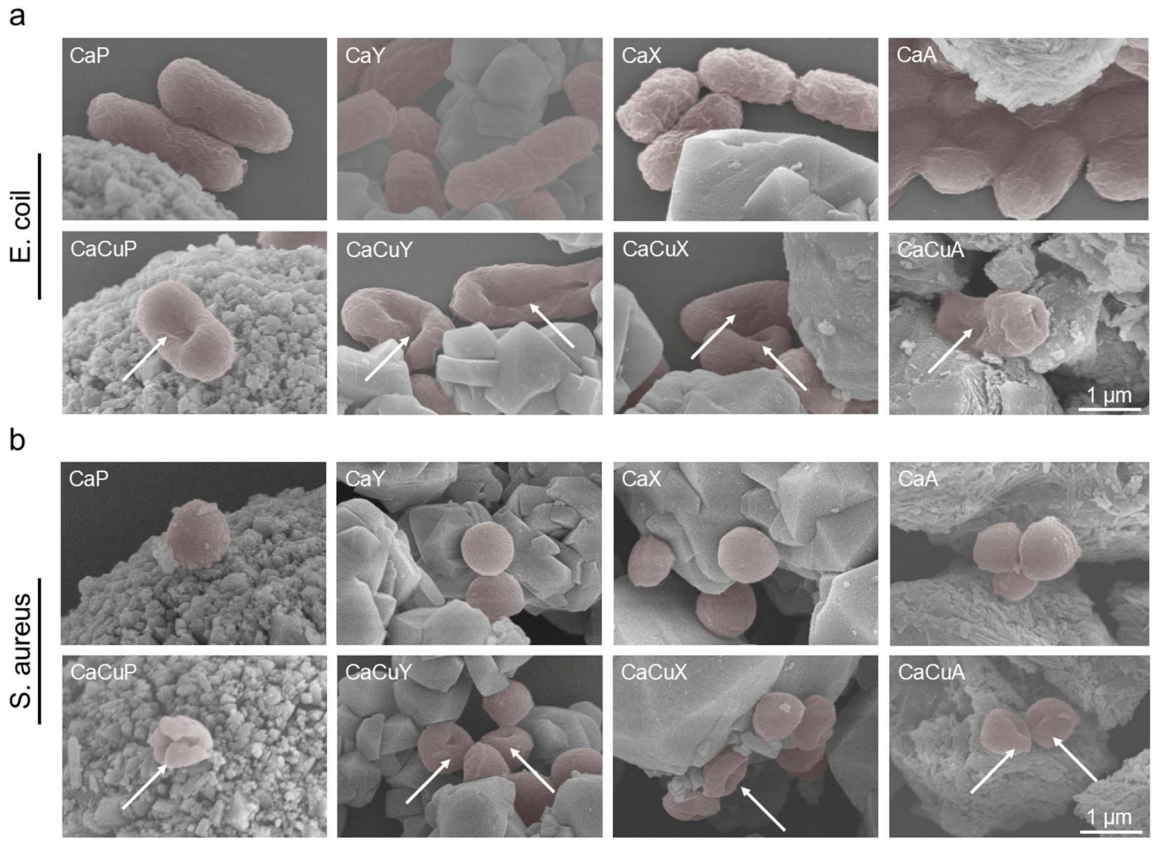

Fig. 5 SEM images of (a) *E. coli* and (b) *S. aureus* treated with CaZ and different CaCuZ materials with a copper content of 6.30 mg g^{-1}. The bacteria appear colored in the images.

and their toxicity (Fig. 6). In general, CaCuA possessed the best biocompatibility, and the cell viability rates of CaCuP and CaCuY were slightly lower than others in the entire range, which can be ascribed to the fewest copper ions released from CaCuA zeolite, as indicated in Fig. 4e. Fortunately, there was no obvious cytotoxicity in both the CaCuY group and the CaCuX group. When the copper contents of CaCuP and CaCuY were less than 6.30 mg g^{-1}, the cell viability rates were still higher than 70%, indicating that the cytotoxicity can be adjusted by controlling the copper amount of the samples. Therefore, when the copper content of CaCuZ materials is controlled at a low level, it does not bring serious side effects when treating wounds.

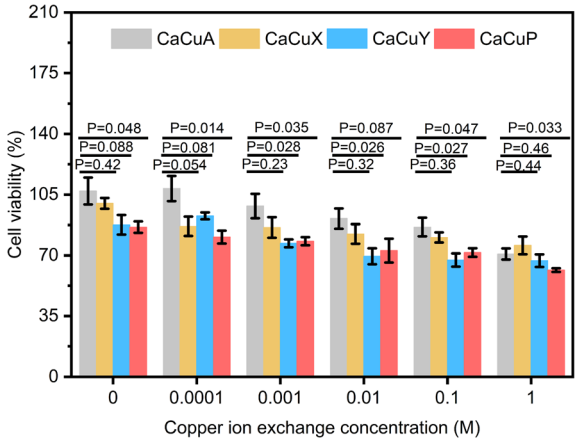

Fig. 6 Cell viability of 3T3 cells cultured with extracts of CaCuZ (adsorption of copper: 6.30 mg g^{-1}), $n = 4$. Error bars, mean ± SEM. The results were analyzed using one-way analysis of variance (ANOVA).

3.7. Discussion

The results of this study show that the copper content has a great influence on the hemostatic performance, antibacterial performance, and cytocompatibility of CaCuZ materials. These experiments indicate that a CaCuZ zeolite that can release more copper ions generally possesses a stronger antibacterial ability, but it will reduce the procoagulation performance and increase the cytotoxicity as well. Copper ions are active ingredients for antibacterial applications, while copper ions are plasma anticoagulants. Fortunately, when the copper content of CaCuP is in the range of 0.64–6.30 mg g^{-1}, CaCuP shows excellent hemostatic properties (<2.5 min), good antibacterial properties (>95%), and good biocompatibility, which achieves a satisfactory balance in these three aspects.

Among the four zeolites, zeolite P is the preferred material because it demonstrates a much better resistance to copper ions in terms of hemostatic property than zeolite Y and X, and its

antibacterial efficiency is significantly higher than zeolite X and zeolite A. It is quite interesting that CaCuP possesses similar copper ion adsorbing and releasing behavior to CaCuY, and they also show similar antibacterial and cytocompatibility properties, which can be explained by their analogous copper ion adsorbing and releasing behavior. However, it shows excellent resistance to copper ions in plasma coagulation, although it will also release a relatively large amount of copper ions into plasma, like CaCuY material, which shows poor resistance to copper ions in plasma coagulation. Meanwhile, although CaCuX releases fewer copper ions, its hemostatic performance is still inferior to that of CaCuP. This result indicates that the release of copper ions into plasma is not the only key reason. It has been reported that the protein corona formed on the surface of zeolite can significantly affect the coagulation cascade process.[25] In terms of hemostatic performance, the protein corona formed on the surface of CaCuP may possess higher resistance to the copper ions. This unique excellent resistance to the copper ions of the CaCuP zeolite needs more in-depth research in the future.

It is widely accepted that metal ions such as copper ions, zinc ions, and silver ions do not cause noteworthy bacterial resistance problems.[28] Therefore, using CaCuZ as a bifunctional material in wound treatment can achieve hemostasis in the first place and prevent the wound from being infected by bacteria at the same time. These CaCuZ hemostatic materials may greatly decrease the possibility of wound bacterial infection without causing the risk of bacterial resistance, which will provide promising benefits in wound treatment.

4. Conclusion

In conclusion, a series of CaCuZ with different zeolite crystal structures and different copper contents were fabricated *via* a two-step ion exchange process by using sodium-based zeolites as their precursors, including NaP, NaY, NaX, and NaA. The introduction of copper ions can enhance the antibacterial performance of zeolite, but it reduces its coagulant-promoting performance and increases its cytotoxicity. The effects of zeolite crystal structure and copper ion content on its hemostatic performance, antibacterial performance, and cytotoxicity are studied. The results show that the material with zeolite P has the best comprehensive performance. When the copper content of CaCuP is in the range of 0.64–6.30 mg g^{-1}, CaCuP has remarkable hemostatic performance (<2.5 min), excellent antibacterial efficiency (>95%) and good biocompatibility. A satisfactory balance in these three aspects is successfully achieved for this material. This bifunctional CaCuP material will provide a new solution for wound treatment.

Data availability

The data supporting this article have been included as part of the ESI.†

Author contributions

Mingtao Wang: conceptualization, methodology, investigation, formal analysis, and writing – original draft. Yifeng Shi: conceptualization, methodology, validation, formal analysis, writing – original draft, and writing – review & editing. Jianrong Huang: methodology and investigation. Liping Xiao: conceptualization, resources, validation, and writing – review & editing. Jie Fan: conceptualization, resources, validation, supervision, funding acquisition, and writing – review & editing.

Conflicts of interest

There are no conflicts to declare.

Acknowledgements

This work was supported by the National Natural Science Foundation of China (92045301, 91845203, 82202483).

References

1 J. Ding, K. Xu, H. Xu, J. Ji, Y. Qian and J. Shen, *Small Struct.*, 2024, **5**, 2300151.
2 Z. Wang, F. Rong, Z. Li, W. Li, K. Kaur and Y. Wang, *Chem. Eng. J.*, 2023, **452**, 139297.
3 S. A. Eming, P. Martin and M. Tomic-Canic, *Sci. Transl. Med.*, 2014, **6**, 265sr6.
4 M. A. Dereli and S. Erdogan, *Transp. Res. A Policy Pract.*, 2017, **103**, 106–117.
5 Y. Yan, L. Chen, L. Zheng, G. Wang, H. Zhang, X. Feng, Y. Liu, L. Li, Y. S. Zhang, P. Ji and X. Zhang, *Adv. Funct. Mater.*, 2024, **34**, 2315590.
6 J. S. Chin, L. Madden, S. Y. Chew and D. L. Becker, *Adv. Drug Deliv. Rev.*, 2019, **149–150**, 2–18.
7 M. Long, Q. Liu, D. Wang, J. Wang, Y. Zhang, A. Tang, N. Liu, B. Bui, W. Chen and H. Yang, *Mater. Today Adv.*, 2021, **12**, 100190.
8 J. W. Cannon, Hemorrhagic Shock, *N. Engl. J. Med.*, 2018, **378**, 370–379.
9 X.-F. Li, P. Lu, H.-R. Jia, G. Li, B. Zhu, X. Wang and F.-G. Wu, *Coord. Chem. Rev.*, 2023, **475**, 214823.
10 A. Simpson, A. Shukla and A. C. Brown, *Annu. Rev. Biomed. Eng.*, 2022, **24**, 111–135.
11 D. A. Hickman, C. L. Pawlowski, U. D. S. Sekhon, J. Marks and A. S. Gupta, *Adv. Mater.*, 2018, **30**, 1700859.
12 S. Zhang, X. Lei, Y. Lv, L. Wang and L.-N. Wang, *Carbohydr. Polym.*, 2024, **327**, 121673.
13 A. Sanyal, S. Roy, A. Ghosh, M. Chakraborty, A. Ghosh and D. Mandal, *Chem. Eng. J.*, 2024, **497**, 155033.
14 R. Zhao, Z. Zhao, S. Song and Y. Wang, *ACS Appl. Mater. Interfaces*, 2023, **15**, 59854–59865.
15 Y. Guo, M. Wang, Q. Liu, G. Liu, S. Wang and J. Li, *Theranostics*, 2023, **13**, 161–196.
16 O. Pinkas, D. Goder, R. Noyvirt, S. Peleg, M. Kahlon and M. Zilberman, *Acta Biomater.*, 2017, **51**, 125–137.

17 M. Liu, Y. Shen, P. Ao, L. Dai, Z. Liu and C. Zhou, *RSC Adv.*, 2014, **4**, 23540–23553.
18 P. Zhao, Y. Feng, Y. Zhou, C. Tan and M. Liu, *Bioact. Mater.*, 2023, **20**, 355–367.
19 Y. Feng, X. Luo, F. Wu, H. Liu, E. Liang, R. He and M. Liu, *Chem. Eng. J.*, 2022, **428**, 132049.
20 X. Lin, Y. Feng, Y. He, S. Ding and M. Liu, *Int. J. Biol. Macromol.*, 2023, **237**, 124148.
21 X. Lin, D. Zhang, X. Chen and M. Liu, *ACS Sustain. Chem. Eng.*, 2024, **12**, 11739–11753.
22 S. Li, J. Li, M. Dong, S. Fan, T. Zhao, J. Wang and W. Fan, *Chem. Soc. Rev.*, 2019, **48**, 885.
23 Y. Liang, C. Xu, F. Liu, S. Du, G. Li and X. Wang, *ACS Appl. Mater. Interfaces*, 2019, **11**, 23848–23857.
24 Y. Li, X. Liao, X. Zhang, G. Ma, S. Zuo, L. Xiao, G. D. Stucky, Z. Wang, X. Chen, X. Shang and J. Fan, *Nano Res.*, 2014, **7**, 1457–1465.
25 X. Shang, H. Chen, V. Castagnola, K. Liu, L. Boselli, V. Petseva, L. Yu, L. Xiao, M. He, F. Wang, K. A. Dawson and J. Fan, *Nat. Catal.*, 2021, **4**, 607–614.
26 H. Brüssow, *Microb. Biotechnol.*, 2024, **17**, e14510.
27 D. Panáček, J. Belza, L. Hochvaldová, Z. Bařdura, G. Zoppellaro, M. Šrejber, T. Malina, V. Šedajová, M. Paloncýová, R. Langer, L. Zdražil, J. Zeng, L. Li, E. Zhao, Z. Chen, Z. Xiong, R. Li, A. Panáček, R. Večeřová, P. Kučová, M. Kolář, M. Otyepka, A. Bakandritsos and R. Zbořil, *Adv. Mater.*, 2024, **36**, 2410652.
28 S. Saidin, M. A. Jumat, N. A. A. M. Amin and A. S. S. Al-Hammadi, *Mater. Sci. Eng. C*, 2021, **118**, 111382.
29 P. Kumari, M. Choudhary, A. Kumar, P. Yadav, B. Singh, R. Kataria and V. Kumar, *Inorg. Chem. Commun.*, 2023, **158**, 111409.
30 I. Salah, I. P. Parkin and E. Allan, *RSC Adv.*, 2021, **11**, 18179.
31 M. Vincent, P. Hartemann and M. Engels-Deutsch, *Int. J. Hyg Environ. Health*, 2016, **219**, 585–591.
32 D. Mitra, E.-T. Kang and K. G. Neoh, *ACS Appl. Mater. Interfaces*, 2020, **12**, 21159–21182.
33 C. Shuai, L. Liu, M. Zhao, P. Feng, Y. Yang, W. Guo, C. Gao and F. Yuan, *J. Mater. Sci. Technol.*, 2018, **34**, 1944–1952.
34 G. Applerot, J. Lellouche, A. Lipovsky, Y. Nitzan, R. Lubart, A. Gedanken and E. Banin, *Small*, 2012, **8**, 3326–3337.
35 M. Li, Z. Ma, Y. Zhu, H. Xia, M. Yao, X. Chu, X. Wang, K. Yang, M. Yang, Y. Zhang and C. Mao, *Adv. Healthc. Mater.*, 2016, **5**, 557–566.
36 Z. Wang, K. Liang, S.-W. Chan and Y. Tang, *J. Hazard. Mater.*, 2019, **371**, 550–557.
37 Q. Lv, B. Zhang, X. Xing, Y. Zhao, R. Cai, W. Wang and Q. Gu, *J. Hazard. Mater.*, 2018, **347**, 141–149.
38 Y. L. Li, D. T. McCarthy and A. Deletic, *J. Hazard. Mater.*, 2014, **273**, 222–230.
39 M. Wang, W. Zhang, C. Wang, L. Xiao, L. Yu and J. Fan, *RSC Adv.*, 2024, **14**, 878.
40 L. Yu, X. Shang, H. Chen, L. Xiao, Y. Zhu and J. Fan, *Nat. Commun.*, 2019, **10**, 1932.
41 X. Chen, L. Yu, S. Zou, L. Xiao and J. Fan, *Sci. Rep.*, 2020, **10**, 4719.
42 C. Wang, C. Shi, J. Huang, X. Wei, Y. Shi, L. Xiao and J. Fan, *ACS Appl. Mater. Interfaces*, 2024, **16**, 49186–49196.
43 S. D. Maat, K. Joseph, C. Maas and A. P. Kaplan, *Clin. Rev. Allergy Immunol.*, 2021, **60**, 348–356.
44 M. M S, D. B. Samal, V. Amirtraj J, S. Subramanian and G. D. Venkatasubbu, *Colloids Surf., B*, 2024, **239**, 113927.
45 E. A. Abou-Shady, H. E. Farrag, N. A. EI-Damarawy, F. A. Mohamed, A. M. Kamel, A. A. Massoud and J. Egypt, *Publ. Health Assoc.*, 1991, **66**, 21–48.
46 J. Fan, X. Qiu, X. Niu, Z. Tian, W. Sun, X. Liu, Y. Li, W. Li and J. Meng, *Mater. Sci. Eng. C*, 2013, **33**, 2345–2352.